






Self-synchronized and cost-effective time-resolved measurements at x-ray free-electron lasers with femtosecond resolution

Philipp Dijkstal ^{1,2} Alexander Malyzhenkov,¹ Paolo Craievich ¹ Eugenio Ferrari,¹ Romain Ganter,¹ Sven Reiche,¹ Thomas Schietinger ¹ Pavle Juranić ¹ and Eduard Prat ^{1,*}

¹Paul Scherrer Institut, CH-5232 Villigen PSI, Switzerland

²Department of Physics, ETH Zürich, 8092 Zürich, Switzerland



(Received 25 August 2021; accepted 29 November 2021; published 7 January 2022)

X-ray free-electron lasers (XFELs), with pulse durations of a few tens of femtoseconds or shorter, are cutting-edge instruments capable of observing structure and dynamics at the atomic scale. Temporal diagnostics are challenging but of fundamental importance for XFEL performance and experiments. In this paper, we demonstrate a method to characterize on a single-shot basis the temporal profile of both the electron beam and the XFEL radiation with femtosecond resolution. The approach consists in streaking the electron beam after the undulator using the wakefields of a corrugated structure. Its merits are arrival time stability and cost-effectiveness. Our method allows access to self-synchronized femtosecond diagnostics to any XFEL facility at low cost.

DOI: [10.1103/PhysRevResearch.4.013017](https://doi.org/10.1103/PhysRevResearch.4.013017)

I. INTRODUCTION

Exploration of matter and its dynamics on subnanometer space and subfemtosecond timescales has become possible by recent progress in x-ray free-electron lasers (XFELs) [1–10]. Identifying the temporal power profile of the XFEL radiation on a shot-to-shot basis is of great importance for user experiments as well as for setup and optimization purposes.

There are different approaches to characterize the XFEL temporal properties. Direct methods based on terahertz/infrared streaking have successfully been demonstrated [11–15] but are extremely challenging, especially for hard x rays due to their weak interaction with matter. Other direct techniques using an optical laser are cross-correlation [16,17] and interferometry [18,19]. A simpler option is to reconstruct the pulse duration from FEL spectral information [20,21]. This indirect method estimates the pulse duration but does not reveal detailed time-resolved information.

Another indirect approach is based on measuring the electron beam. The FEL process results in an average energy loss and an energy spread increase of the lasing parts or slices of the beam. Therefore, comparing the longitudinal phase space of the electrons (i.e., the energy properties as a function of time) with and without lasing condition allows the retrieval of the temporal profile of the x rays. The longitudinal phase space is reconstructed by measuring the transverse beam distribution: the time information is obtained by streaking the

beam (i.e., imposing a time-dependent kick) in one transverse plane after the undulator, while the energy properties are accessible via dispersion in the other transverse direction. This method has been demonstrated at the Linac Coherent Light Source (LCLS) [22] using an X-band (~ 12 GHz) radio-frequency (rf) transverse deflector (TD) for streaking. TDs are routinely used in linear accelerators for temporal diagnostics of electron beams [22–31].

In this paper, we demonstrate the single-shot temporal power profile measurement of XFEL pulses with femtosecond resolution by using a post-undulator passive wakefield streaker instead of a TD. An electron beam traveling off axis through such a device excites transverse wakefields, resulting in a time-dependent kick that streaks the electron beam. We use a metallic corrugated structure [32,33], but one could also employ a dielectric structure [34,35] for this task. The experiments were carried out at SwissFEL [10].

Our procedure based on passive streaking has two main advantages in comparison to the TD approach. First, the passive streaking method is self-synchronized, thus stable in terms of arrival time jitter. By contrast, the time jitter is an important limitation of TD-based measurements and requires exquisite synchronization between the beam arrival time and the driving rf phase. Second, the passive system is much less complex and the hardware and operational costs are substantially reduced. As an example, the C-band (~ 6 GHz) system used at SwissFEL [28] costs ~ 2.4 one million (1e6) Swiss Franc and its maximum power consumption is 75 kW, while the corrugated structure used for the experiments presented here cost ~ 110 one thousand (1e3) Swiss Francs and consumes no power.

The passive streaking method has, however, some drawbacks in comparison to the TD. The streaking is nonlinear, resulting in a nonconstant resolution along the bunch, where the bunch head cannot be fully resolved. The nonlinear streaking requires a complex algorithm to retrieve the relation

*eduard.prat@psi.ch

Published by the American Physical Society under the terms of the [Creative Commons Attribution 4.0 International license](https://creativecommons.org/licenses/by/4.0/). Further distribution of this work must maintain attribution to the author(s) and the published article's title, journal citation, and DOI.

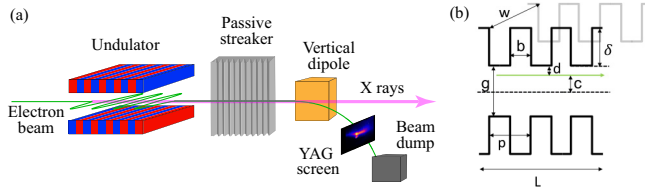


FIG. 1. (a) Layout of the post-undulator electron and photon beam diagnostics with a corrugated passive structure. (b) Schematic of the geometry of the structure (not to scale) with parameters total length $L = 1$ m, plate width $w = 40$ mm, corrugation depth $\delta = 250$ μm , and period $p = 500$ μm , longitudinal gap $b = 250$ μm , and variable gap $g \leq 28$ mm. The horizontal position of the streaker center (relative to the beam) c and the gap define the distance between the beam and the plate: $d = g/2 - c$.

between the time and transverse coordinates of the beam. Furthermore, the streaking strength is sensitive to structure tilts and orbit jitter [36], although the latter can be accounted for by measuring the electron beam trajectory with standard diagnostics.

The utilization of passive structures to reconstruct the temporal properties of electron beams was proposed and demonstrated with a dielectric device at a relatively low beam energy (140 MeV) and ~ 10 fs resolution [37], and later with a corrugated structure with a similar beam energy (70 MeV) [38]. Here we further advance the method, demonstrating its capability to measure electron beams at higher energies (6 GeV) with femtosecond resolution, and, most importantly, showing that it can be used to obtain the temporal profile of XFEL pulses. The wakefields of passive structures have found other applications in XFEL facilities, such as tailoring the energy chirp of electron beams [35,39,40], streaking the electron beam upstream of the undulator to produce short and high-power XFEL radiation [41], and generating two-color XFEL pulses [42].

Figure 1 shows a sketch of the experimental setup and the geometry of the corrugated structure. The 1-m aluminum device consists of two horizontally movable plates with vertical corrugation. Stepper motors (one for each plate) control the gap and the relative offset of the streaker with submicrometer precision. For the measurements presented here, the gap g was set to 10 mm. After being streaked horizontally, the electron beam is observed with a scintillator screen [43] at the dump, a location with vertical dispersion, thus allowing the measurement of the longitudinal phase space of the electrons. A C-band TD located upstream of the undulator is used to benchmark the current profile reconstruction with the passive streaker.

II. RECONSTRUCTION OF THE ELECTRON BEAM CURRENT PROFILE

The single-particle wakefields [33] describe the action of a leading particle on a trailing electron through interaction with the streaker plates. They can be computed from the parameters shown in Fig. 1(b). Longitudinal wakefields affect the beam energy, whereas transverse wakefields change the beam trajectory. The transverse wakefield model includes dipole and

quadrupole components, resulting in streaking and defocusing effects, respectively.

The time-dependent kick $\Delta x'(t)$ imposed by the passive streaker is found numerically as a convolution of the single-particle wakefield and the electron beam current distribution $I(t)$. After the streaker, $\Delta x'(t)$ is converted to a time-dependent horizontal position change on the screen $\Delta x(t) = R_{12}\Delta x'(t)$, where R_{12} is the linear beam transport matrix element between the streaker and the screen.

The reconstruction of the current profile, $I(t)$, from the horizontal distribution at the screen, $\rho(x)$, is an implicit problem, as the streaking depends on $I(t)$ itself, and calls for a multistep procedure. We apply the following algorithm:

(1) Calculate $\Delta x'(t)$ assuming a Gaussian current profile with rms (root mean square) duration σ .

(2) Obtain $\Delta x(t)$, invert it to get $t(x)$, and transform $\rho(x)$ to obtain an intermediate reconstructed current $I_R^*(t)$.

(3) Repeat steps 1 and 2 using $I_R^*(t)$ for an improved wakefield estimation, and obtain the final reconstructed current $I_R(t)$ (for a given σ).

(4) Forward propagate $I_R(t)$ to get the final reconstructed horizontal projection $\rho_R(x)$:

(a) Randomly generate three-dimensional macroparticles (x, x', t) , where the t distribution follows I_R , and where the x, x' distributions are Gaussian and follow the assumed transverse beam optics and emittance.

(b) Apply $\Delta x'(t)$ at the streaker and propagate the beam to the screen to obtain the reconstructed screen distribution $\rho_R(x)$.

(5) Repeat steps 1–4 for different σ , and select $I_R(t)$ for which the weighted average $\langle x \rangle_{\rho_R}$ (the reconstructed beam centroid) is in best agreement with the measured $\langle x \rangle_{\rho}$.

For the forward propagation [step (4)], the beam is represented as a distribution with 10^5 macroparticles in x, x', t coordinates. The streaker is modeled as two drift spaces of half length, with the x' coordinates being changed in between according to the transverse dipole wake potential. Linear beam transport matrices are used to represent all other elements between the passive streaker and the beam screen. For backward propagation, only the horizontal coordinate x is used, which is then converted to t . The current profile (after backward propagation) and transverse charge distributions (after forward propagation) are obtained by taking the histograms in the respective coordinates, t or x . For the procedure, only the linear beam transport matrix between the passive streaker and the screen is required.

The beam orbit and bunch duration jitters at the streaker location cause a difference in streaking strength between shots. In our case, according to our TD measurements, the orbit variation is dominant over the bunch duration jitter. To overcome this jitter effect we take multiple images for the same streaking configuration and perform the analysis only for the image with the median value of $\langle x \rangle_{\rho}$. A better way to correct for jitter (not yet attempted) would be based on measuring the electron beam trajectory on a shot-to-shot basis with beam-position monitors. The calculations only include the dipole wakefield component, since the quadrupole term depends on the horizontal particle coordinates at the streaker location, and thus cannot easily be accounted for in the second step of the above procedure.

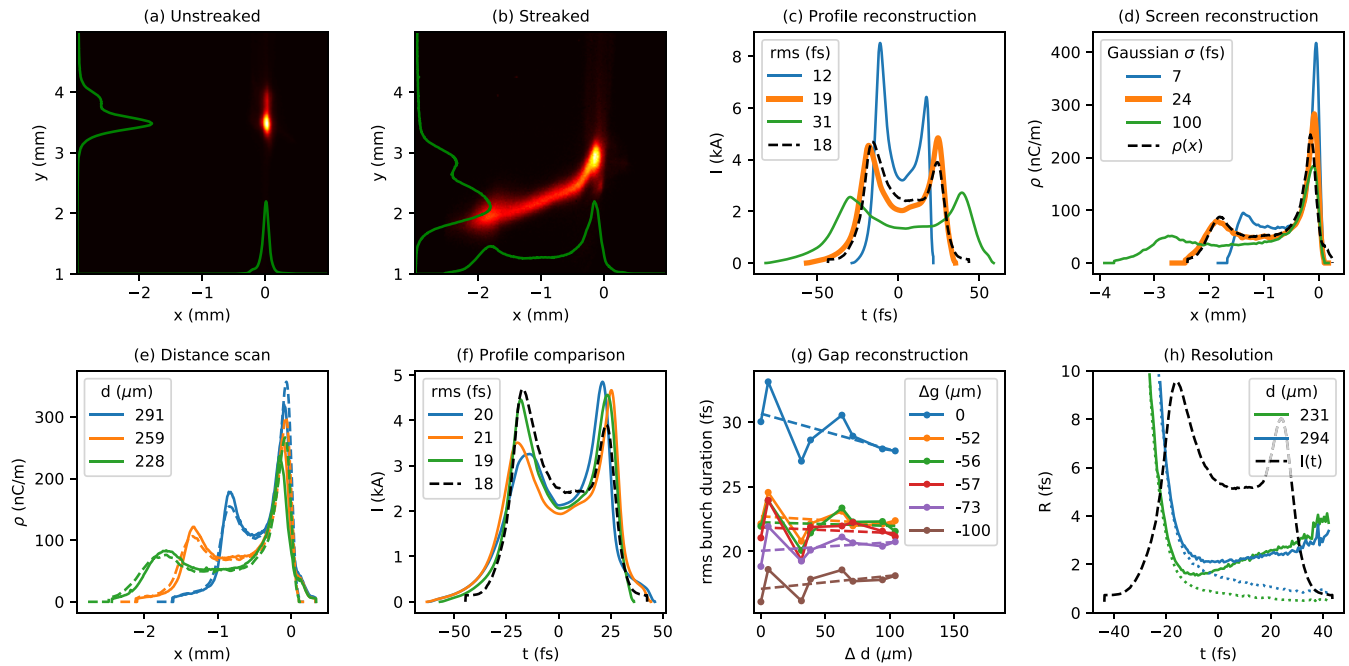


FIG. 2. Reconstruction of electron beam current profile. (a),(b) Single-shot images of unstreaked and streaked electron beams. (c) TD measured profile (black) and reconstructed profiles for different initial Gaussian distributions I_R (color). The current profile reconstruction algorithm converges at the orange profile. (d) Measured horizontal image projection ρ (black) and forward propagated ρ_R (color) corresponding to the profiles I_R in (c). (e) Measured (solid) and reconstructed (dashed) image projections for different positions of the passive staker. (f) Reconstructed current profiles corresponding to the horizontal projections in (e). For comparison, the TD measured profile is shown in black. (g) Reconstructed electron bunch durations for different staker positions (horizontal axis) and under different gap corrections (solid), with linear fits (dashed). (h) Calculated time resolution of the passive staker, using the TD measured time profile (black, arb. units), for two different gaps, with (solid) and without (dotted) quadrupole field effects. See text for further details.

Our algorithm is very sensitive to the distance between the beam and the plate d . A wrong assumption on d will result in a reconstructed current profile of wrong duration despite good agreement in the horizontal projections. Therefore, the gap and the structure center position need to be well known. We find the structure center by measuring the electron beam centroids at the screen for different staker positions [44]. To calibrate the gap we exploit the condition that the reconstructed current profile should not significantly change when the staker center position is varied within certain limits.

Following the above strategy, we have demonstrated the current profile reconstruction of bunches with 180 pC charge and 6 GeV beam energy at SwissFEL (see Fig. 2). The horizontal phase advance between the staker center and the screen was set to 62° . Single-shot images are shown without (a) and with (b) streaking. The transverse staker wakefields spread the beam horizontally, while the longitudinal wakefields cause an energy loss along the bunch, manifest on the vertical screen axis. The unstreaked and streaked horizontal rms beam sizes are ~ 75 and ~ 700 μm , respectively, corresponding to a streaking factor of about 10. The distance between the beam and the staker plate is 231 μm in the example of Fig. 2(b).

Plots (c) and (d) illustrate the current profile reconstruction for the image in (b). Some current profiles (I_R) and screen projections (ρ_R) of the algorithm discussed above are shown for values of σ ranging between 7 and 75 fs. The algorithm converges to a current profile with an rms pulse duration of 18 fs, which is very similar to the profile obtained from an inde-

pendent TD measurement performed immediately afterwards under the same machine settings (c). The measured screen projection agrees well with the final computed distribution (d).

The following plots contain screen distributions (e) and current profiles (f) for three different distances between beam and plate (231, 263, 294 μm). Again we find good agreement between the measured and forward propagated horizontal beam projections at the screen, as well as between the current profiles measured with the TD and with the passive staker.

The staker gap calibration is shown in Fig. 2(g): After measuring current profiles at eight different staker positions, giving streaking factors between 2.8 and 9.0, and reconstructing the corresponding bunch durations assuming different gap values, we identify the most probable gap value as the one that minimizes the linear correlation between rms bunch durations and staker positions. If no gap correction is applied ($\Delta g = 0$) the measurements indicate a clear correlation between reconstructed bunch durations and staker positions, as well as an overestimation of the bunch duration in comparison to the TD measurement. Our calibration procedure indicates a gap reduction of 57 μm , which is used for all other results presented here. (A reduction of the geometrical gap by ~ 100 μm was found in previous studies for similar corrugated structures [44].) The statistical error in rms duration of the reconstructed profiles for different staker positions (using the corrected gap) is ~ 1 fs.

Figure 2(h) shows the estimated time resolution [45] of the reconstructed current profiles for two distances to the plate (294 and 231 μm), with and without quadrupole field effects.

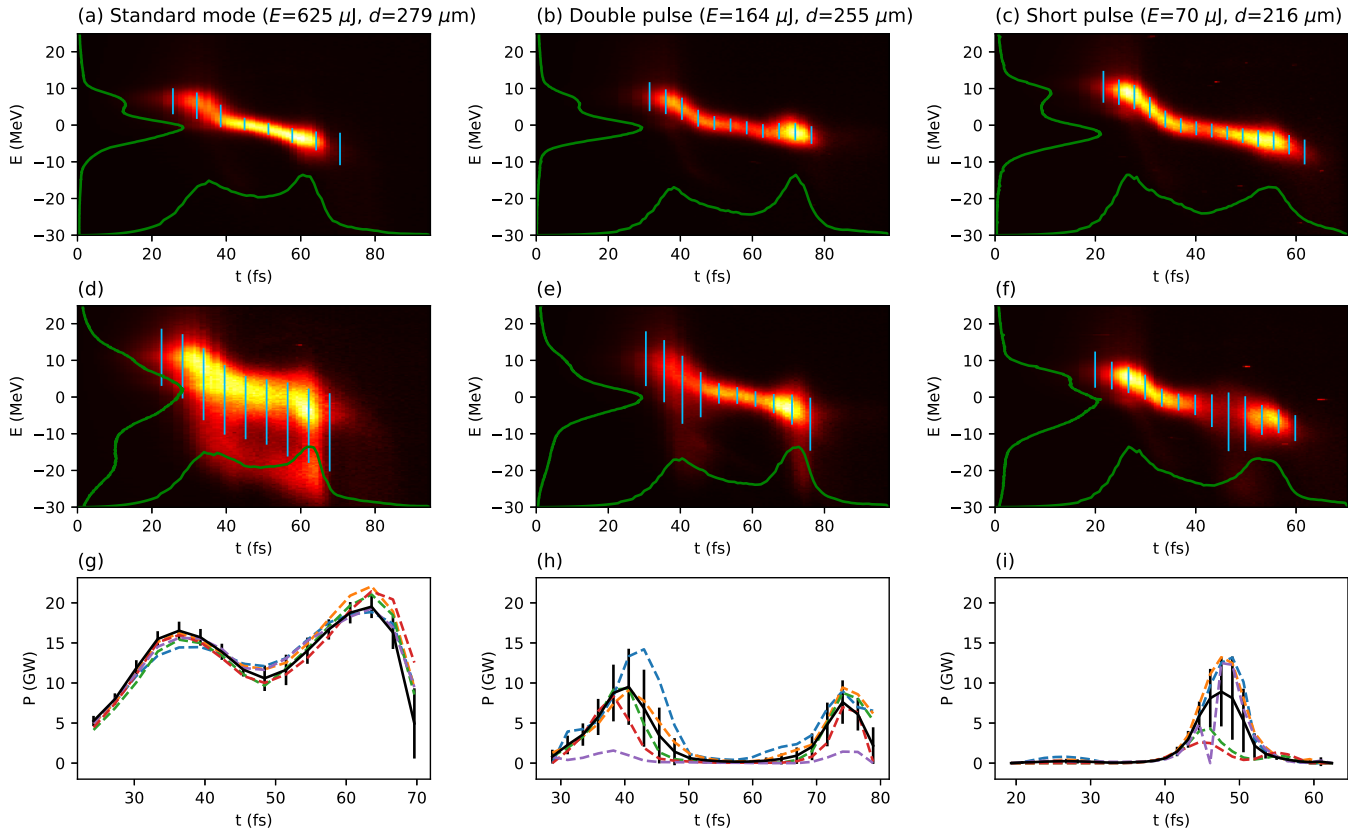


FIG. 3. FEL power profile reconstruction. Top and middle row: Longitudinal electron beam phase-space distributions with lasing off (top) and lasing on (middle) for different machine configurations: standard mode (a),(d), two-pulse mode (b),(e) and short-pulse mode (c),(f). The average pulse energies (E) and the distances between beam and stalker plate (d) are indicated at the top. The rms widths around the slice centroids are shown in blue. The projections onto both axes are shown in green. Bottom row: reconstructed average FEL power profiles (black) and single-shot examples (color) for standard mode (g), two-pulse mode (h), and short-pulse mode (i).

The resolution is calculated from a forward propagation of the TD measured profile [see step (4) of the algorithm above]. The quadrupole effects are highly sensitive to the transverse beam size at the passive stalker location. We estimate the beam size to be $11 \mu\text{m}$ at the stalker from design optics and assuming an emittance of 200 nm , consistent with the measurements presented in [46]. The estimated resolution is below 2 fs for most of the bunch when only considering the dipole field component, and between 2 and 3 fs when including quadrupole wakefield effects. Future studies to improve the resolution will focus on optimizing the beam optics, as suggested in [45].

III. RECONSTRUCTION OF THE FEL POWER PROFILE

Having demonstrated the ability to retrieve the electron beam current profile, we proceed with the reconstruction of the FEL power profile $P(t)$. It can be obtained from longitudinal electron beam phase-space measurements in two different ways. First using $P(t) = \Delta E(t)I(t)/e$, where ΔE is the slice energy loss due to lasing, and e the electron charge. Second from the changes in the slice energy spread between lasing-on (σ_{on}) and lasing-off conditions (σ_{off}), according to $P(t) \propto [\sigma_{\text{on}}(t)^2 - \sigma_{\text{off}}(t)^2]I(t)^{2/3}$ [22,47]. The absolute pulse energy calibration required for the second method can be obtained by integration of the power profile using the first approach, or by an independent photon pulse energy mea-

surement. The first method is sensitive to central beam energy and energy chirp jitter, significant in our setup, hence we only show the relatively more robust approach based on the slice energy spread. We suppress lasing by slightly detuning the field strengths of the undulator modules, which is sufficient to stop the FEL process while maintaining equivalent optics and impact of the undulator wakefields on the electron beam.

The longitudinal phase space is obtained from camera images by inversion of the nonlinear $x(t)$ relation as described above, and by using the dispersion function to convert the vertical coordinate y to beam energy ΔE . We then divide the phase space into temporal slices, and calculate the rms energy spread for those slices with sufficient contrast for a stable result (typical cutoff at around 20% of the maximum intensity). Single-shot power profiles are calculated using the corresponding lasing-on phase space and the average phase-space properties of the lasing-off configuration.

As mentioned earlier, horizontal trajectory jitter at the stalker location causes a significant difference in streaking strength between shots, and needs correction. We perform a current profile reconstruction for each horizontal image projection $\rho(x)$ and define the profile $I(t)$ belonging to the median value of $\langle x \rangle_\rho$ as being valid for all shots. The differences in $\langle x \rangle_\rho$ between shots are attributed to orbit jitter, and are used to fit corrections of the beam position. The wakefields required for the transformation of x to t are obtained using

the updated beam positions. The corrections for the examples shown later are usually between $\pm 10 \mu\text{m}$ and compensate differences in measured rms beam size of about $\pm 10\%$ (full width in both cases).

We demonstrate the FEL power profile reconstruction for three different operation modes achieved at a photon energy of 11.3 keV: (1) standard mode with maximum pulse energy; (2) double-pulse operation using a second-order horizontal beam tilt induced with a sextupole magnet [48]; and (3) short-pulse operation using a vertical beam tilt induced with a passive wakefield device installed upstream of the undulator [41]. In our analysis of cases 2 and 3 we assume that the wakefield model [33] holds for transversely tilted electron beams.

The results are displayed in Fig. 3. The upper and middle plots depict reconstructed single-shot longitudinal phase-space distributions for lasing-off and lasing-on conditions. A visual comparison of the images clearly shows that lasing slices lose energy and exhibit an increased energy spread. The average FEL power profile over 20 measurements and a few single-shot examples are shown for each setting. The error bars of the average power profile correspond to the statistical uncertainties from all corresponding single-shot power profiles. We determine the calibration factor required for $P_\sigma(t)$ from the average power profile for the full lasing configuration, and the corresponding average pulse energy measured with a gas detector monitor [49]. This calibration is then applied to the individual power profiles for all configurations.

The standard mode (Fig. 3, left) exhibits an average pulse energy of approximately $625 \mu\text{J}$, and an rms pulse duration of 13 fs, as measured with our method. In the double-pulse mode the rms pulse durations, obtained from Gaussian fits, are about 3.3 fs and 3.6 fs, with a separation of about 35 fs in between. The duration of the FEL pulse in the short-pulse mode (Fig. 3 right) is about 2.8 fs. The reconstructed pulse

durations for the double- and short-pulse cases are close to the calculated resolution shown in Fig. 2(b). In both special modes, undesired lasing from other parts of the bunch is well suppressed.

IV. CONCLUSIONS

In conclusion, we have demonstrated a method to measure the electron beam current distribution and the FEL radiation power profile with femtosecond resolution and single-shot capability. The approach is based on streaking the electron beam after the undulator beam line using the wakefields of a corrugated structure, and does not require calibration by means of an independent bunch-profile measurement. In comparison to the established method based on a TD, the advantages of our approach are robustness against arrival-time jitter and cost. The method can readily be implemented at any XFEL beam line by installing a corrugated or dielectric streaker downstream from the undulator section. The acquired shot-to-shot information on the FEL power profile not only expedites setup and optimization of the FEL performance, but may also be of considerable benefit to user experiments.

The raw data used for Figs. 2 and 3 is provided in Ref. [50].

ACKNOWLEDGMENTS

We thank Peter Heimgartner for the mechanical design of the structure, Niko Kivel for the control integration, and Marco Schneider for the mechatronics. We also thank all technical and operation teams at SwissFEL involved in the setup and experiments. The work of P.D. in the context of this project was supported by the Swiss National Science Foundation under Grant No. 200021_175498.

-
- [1] Z. Huang and K.-J. Kim, Review of x-ray free-electron laser theory, *Phys. Rev. ST Accel. Beams* **10**, 034801 (2007).
 - [2] B. W. J. McNeil and N. R. Thompson, X-ray free-electron lasers, *Nat. Photonics* **4**, 814 (2010).
 - [3] C. Pellegrini, A. Marinelli, and S. Reiche, The physics of x-ray free-electron lasers, *Rev. Mod. Phys.* **88**, 015006 (2016).
 - [4] W. Ackermann, G. Asova, V. Ayvazyan, A. Azima, N. Baboi, J. Bähr, V. Balandin, B. Beutner, A. Brandt, A. Bolzmann, R. Brinkmann, O. I. Brovko, M. Castellano, P. Castro, L. Catani, E. Chiadroni, S. Choroba, A. Cianchi, J. T. Costello, D. Cubaynes *et al.*, Operation of a free-electron laser from the extreme ultraviolet to the water window, *Nat. Photonics* **1**, 336 (2007).
 - [5] P. Emma, R. Akre, J. Arthur, R. Bionta, C. Bostedt, J. Bozek, A. Brachmann, P. Bucksbaum, R. Coffee, F.-J. Decker, Y. Ding, D. Dowell, S. Edstrom, A. Fisher, J. Frisch, S. Gilevich, J. Hastings, G. Hays, P. Hering, Z. Huang *et al.*, First lasing and operation of an ångström-wavelength free-electron laser, *Nat. Photonics* **4**, 641 (2010).
 - [6] E. Allaria, D. Castronovo, P. Cinquegrana, P. Craievich, M. D. Forno, M. B. Danailov, G. D'Auria, A. Demidovich, G. D. Ninno, S. D. Mitri, B. Diviacco, W. M. Fawley, M. Ferianis, E. Ferrari, L. Froehlich, G. Gaio, D. Gauthier, L. Giannessi, R. Ivanov, B. Mahieu *et al.*, Two-stage seeded soft-x-ray free-electron laser, *Nat. Photonics* **7**, 913 (2013).
 - [7] T. Ishikawa, H. Aoyagi, T. Asaka, Y. Asano, N. Azumi, T. Bizen, H. Ego, K. Fukami, T. Fukui, Y. Furukawa, S. Goto, H. Hanaki, T. Hara, T. Hasegawa, T. Hatsui, A. Higashiya, T. Hirono, N. Hosoda, M. Ishii, T. Inagaki *et al.*, A compact X-ray free-electron laser emitting in the sub-ångström region, *Nat. Photonics* **6**, 540 (2012).
 - [8] H.-S. Kang, C.-K. Min, H. Heo, C. Kim, H. Yang, G. Kim, I. Nam, S. Y. Baek, H.-J. Choi, G. Mun, B. R. Park, Y. J. Suh, D. C. Shin, J. Hu, J. Hong, S. Jung, S.-H. Kim, K. Kim, D. Na, S. S. Park *et al.*, Hard X-ray free-electron laser with femtosecond-scale timing jitter, *Nat. Photonics* **11**, 708 (2017).
 - [9] W. Decking, S. Abeghyan, P. Abramian, A. Abramsky, A. Aguirre, C. Albrecht, P. Alou, M. Altarelli, P. Altmann, K. Amyan, V. Anashin, E. Apostolov, K. Appel, D. Auguste, V. Ayvazyan, S. Baark, F. Babies, N. Baboi, P. Bak, V. Balandin *et al.*, A MHz-repetition-rate hard x-ray free-electron laser driven by a superconducting linear accelerator, *Nat. Photonics* **14**, 391 (2020).

- [10] E. Prat, R. Abela, M. Aiba, A. Alarcon, J. Alex, Y. Arbelo, C. Arrell, V. Arsov, C. Bacellar, C. Beard, P. Beaud, S. Bettoni, R. Biffiger, M. Bopp, H.-H. Braun, M. Calvi, A. Cassar, T. Celcer, M. Chergui, P. Chevtsov *et al.*, A compact and cost-effective hard x-ray free-electron laser driven by a high-brightness and low-energy electron beam, *Nat. Photonics* **14**, 748 (2020).
- [11] U. Frühling, M. Wieland, M. Gensch, T. Gebert, B. Schütte, M. Krikunova, R. Kalms, F. Budzyn, O. Grimm, J. Rossbach, E. Plönjes, and M. Drescher, Single-shot terahertz-field-driven x-ray streak camera, *Nat. Photonics* **3**, 523 (2009).
- [12] I. Grguraš, A. R. Maier, C. Behrens, T. Mazza, T. J. Kelly, P. Radcliffe, S. Düsterer, A. K. Kazansky, N. M. Kabachnik, T. Tschentscher, J. T. Costello, M. Meyer, M. C. Hoffmann, H. Schlarb, and A. L. Cavalieri, Ultrafast x-ray pulse characterization at free-electron lasers, *Nat. Photonics* **6**, 852 (2012).
- [13] W. Helml, A. R. Maier, W. Schweinberger, I. Grguraš, P. Radcliffe, G. Doumy, C. Roedig, J. Gagnon, M. Messerschmidt, S. Schorb, C. Bostedt, F. Grüner, L. F. DiMauro, D. Cubaynes, J. D. Bozek, T. Tschentscher, J. T. Costello, M. Meyer, R. Coffee, S. Düsterer *et al.*, Measuring the temporal structure of few-femtosecond free-electron laser x-ray pulses directly in the time domain, *Nat. Photonics* **8**, 950 (2014).
- [14] N. Hartmann, G. Hartmann, R. Heider, M. S. Wagner, M. Ilchen, J. Buck, A. O. Lindahl, C. Benko, J. Grünert, J. Krzywinski, J. Liu, A. A. Lutman, A. Marinelli, T. Maxwell, A. A. Miahnahri, S. P. Moeller, M. Planas, J. Robinson, A. K. Kazansky, N. M. Kabachnik *et al.*, Attosecond time-energy structure of x-ray free-electron laser pulses, *Nat. Photonics* **12**, 215 (2018).
- [15] J. Duris, S. Li, T. Driver, E. G. Champenois, J. P. MacArthur, A. A. Lutman, Z. Zhang, P. Rosenberger, J. W. Aldrich, R. Coffee, G. Coslovich, F.-J. Decker, J. M. Glowina, G. Hartmann, W. Helml, A. Kamalov, J. Knurr, J. Krzywinski, M.-F. Lin, J. P. Marangos *et al.*, Tunable isolated attosecond x-ray pulses with gigawatt peak power from a free-electron laser, *Nat. Photonics* **14**, 30 (2019).
- [16] S. Düsterer, P. Radcliffe, C. Bostedt, J. Bozek, A. L. Cavalieri, R. Coffee, J. T. Costello, D. Cubaynes, L. F. DiMauro, Y. Ding, G. Doumy, F. Grüner, W. Helml, W. Schweinberger, R. Kienberger, A. R. Maier, M. Messerschmidt, V. Richardson, C. Roedig, T. Tschentscher *et al.*, Femtosecond x-ray pulse length characterization at the linac coherent light source free-electron laser, *New J. Phys.* **13**, 093024 (2011).
- [17] P. Finetti, H. Höppner, E. Allaria, C. Callegari, F. Capotondi, P. Cinquegrana, M. Coreno, R. Cucini, M. B. Danailov, A. Demidovich, G. De Ninno, M. Di Fraia, R. Feifel, E. Ferrari, L. Fröhlich, D. Gauthier, T. Golz, C. Grazioli, Y. Kai, G. Kurdi *et al.*, Pulse Duration of Seeded Free-Electron Lasers, *Phys. Rev. X* **7**, 021043 (2017).
- [18] O. Y. Gorobtsov, N. Mukharamova, S. Lazarev, M. Chollet, D. Zhu, Y. Feng, R. P. Kurta, J.-M. Meijer, G. Williams, M. Sikorski, S. Song, D. Dzhigaev, S. Serkez, A. Singer, A. V. Petukhov, and I. A. Vartanyants, Diffraction based Hanbury Brown and Twiss interferometry at a hard x-ray free-electron laser, *Sci. Rep.* **8**, 2219 (2018).
- [19] R. Khubbutdinov, N. Gerasimova, G. Mercurio, D. Assalauova, J. Carnis, L. Gelisio, L. L. Guyader, A. Ignatenko, Y. Y. Kim, B. E. V. Kuiken, R. P. Kurta, D. Lapkin, M. Teichmann, A. Yaroslavtsev, O. Gorobtsov, A. P. Menushenkov, M. Scholz, A. Scherz, and I. A. Vartanyants, High spatial coherence and short pulse duration revealed by the Hanbury Brown and Twiss interferometry at the european XFEL, *Struct. Dyn.* **8**, 044305 (2021).
- [20] Y. Inubushi, K. Tono, T. Togashi, T. Sato, T. Hatsui, T. Kameshima, K. Togawa, T. Hara, T. Tanaka, H. Tanaka, T. Ishikawa, and M. Yabashi, Determination of the Pulse Duration of an X-Ray Free Electron Laser Using Highly Resolved Single-Shot Spectra, *Phys. Rev. Lett.* **109**, 144801 (2012).
- [21] A. A. Lutman, Y. Ding, Y. Feng, Z. Huang, M. Messerschmidt, J. Wu, and J. Krzywinski, Femtosecond x-ray free electron laser pulse duration measurement from spectral correlation function, *Phys. Rev. ST Accel. Beams* **15**, 030705 (2012).
- [22] C. Behrens, F.-J. Decker, Y. Ding, V. A. Dolgashev, J. Frisch, Z. Huang, P. Krejcik, H. Loos, A. Lutman, T. J. Maxwell, J. Turner, J. Wang, M.-H. Wang, J. Welch, and J. Wu, Few-femtosecond time-resolved measurements of x-ray free-electron lasers, *Nat. Commun.* **5**, 3762 (2014).
- [23] I. Ben-Zvi, J. Qiu, and X. Wang, Picosecond-resolution ‘slice’ emittance measurement of electron-bunches, in *Proceedings of PAC 1997, Vancouver, Canada* (IEEE, New York, 1998).
- [24] P. Emma, J. Frisch, and P. Krejcik, A transverse rf deflecting structure for bunch length and phase space diagnostics, LCLS Report No. LCLS-TN-00-12, 2000, <https://www-ssl.slac.stanford.edu/lcls/technotes/LCLS-TN-00-12.pdf>.
- [25] D. Alesini, G. D. Pirro, L. Ficcadenti, A. Mostacci, L. Palumbo, J. Rosenzweig, and C. Vaccarezza, RF deflector design and measurements for the longitudinal and transverse phase space characterization at SPARC, *Nucl. Instrum. Methods Phys. Res., Sect. A* **568**, 488 (2006).
- [26] M. Röhrs, C. Gerth, H. Schlarb, B. Schmidt, and P. Schmöser, Time-resolved electron beam phase space tomography at a soft x-ray free-electron laser, *Phys. Rev. ST Accel. Beams* **12**, 050704 (2009).
- [27] Y. Ding, C. Behrens, P. Emma, J. Frisch, Z. Huang, H. Loos, P. Krejcik, and M.-H. Wang, Femtosecond x-ray pulse temporal characterization in free-electron lasers using a transverse deflector, *Phys. Rev. ST Accel. Beams* **14**, 120701 (2011).
- [28] P. Craievich, R. Ischebeck, F. Löhl, G. L. Orlandi, and E. Prat, Transverse Deflecting Structures for Bunch Length and Slice Emittance Measurements on SwissFEL, in *Proceedings of FEL 2013 (JACoW Geneva, 2013)*, pp. 236–241.
- [29] V. A. Dolgashev, G. Bowden, Y. Ding, P. Emma, P. Krejcik, J. Lewandowski, C. Limborg, M. Litos, J. Wang, and D. Xiang, Design and application of multimegawatt x-band deflectors for femtosecond electron beam diagnostics, *Phys. Rev. ST Accel. Beams* **17**, 102801 (2014).
- [30] H. Ego, H. Maesaka, T. Sakurai, Y. Otake, T. Hashirano, and S. Miura, Transverse C-band deflecting structure for longitudinal electron-bunch-diagnosis in XFEL “SACLA”, *Nucl. Instrum. Methods Phys. Res., Sect. A* **795**, 381 (2015).
- [31] P. Craievich, M. Bopp, H.-H. Braun, A. Citterio, R. Fortunati, R. Ganter, T. Kleeb, F. Marcellini, M. Pedrozzi, E. Prat, S. Reiche, K. Rolli, R. Sieber, A. Grudiev, W. L. Millar, N. Catalan-Lasheras, G. McMonagle, S. Pitman, V. del Pozo Romano, K. T. Szypula *et al.*, Novel X-band transverse deflection structure with variable polarization, *Phys. Rev. Accel. Beams* **23**, 112001 (2020).
- [32] K. L. F. Bane and G. Stupakov, Corrugated pipe as a beam dechirper, *Nucl. Instrum. Methods Phys. Res., Sect. A* **690**, 106 (2012).

- [33] K. Bane, G. Stupakov, and I. Zagorodnov, Analytical formulas for short bunch wakes in a flat dechirper, *Phys. Rev. Accel. Beams* **19**, 084401 (2016).
- [34] M. Rosing and J. Simpson, Passive momentum spread reduction, the Wakefield silencer, ANL Report No. WF-144 (1990).
- [35] S. Antipov, S. Baturin, C. Jing, M. Fedurin, A. Kanareykin, C. Swinson, P. Schoessow, W. Gai, and A. Zholents, Experimental Demonstration of Energy-Chirp Compensation by a Tunable Dielectric-Based Structure, *Phys. Rev. Lett.* **112**, 114801 (2014).
- [36] K. Bane, M. Guetg, and A. Lutman, Wake measurements of a dechirper jaw with nonzero tilt angle, *Phys. Rev. Accel. Beams* **21**, 054402 (2018).
- [37] S. Bettoni, P. Craievich, A. A. Lutman, and M. Pedrozzi, Temporal profile measurements of relativistic electron bunch based on wakefield generation, *Phys. Rev. Accel. Beams* **19**, 021304 (2016).
- [38] J. Seok, M. Chung, H.-S. Kang, C.-K. Min, and D. Na, Use of a corrugated beam pipe as a passive deflector for bunch length measurements, *Phys. Rev. Accel. Beams* **21**, 022801 (2018).
- [39] P. Emma, M. Venturini, K. L. F. Bane, G. Stupakov, H.-S. Kang, M. S. Chae, J. Hong, C.-K. Min, H. Yang, T. Ha, W. W. Lee, C. D. Park, S. J. Park, and I. S. Ko, Experimental Demonstration of Energy-Chirp Control in Relativistic Electron Bunches Using a Corrugated Pipe, *Phys. Rev. Lett.* **112**, 034801 (2014).
- [40] G. Penco, E. Allaria, I. Cudin, S. Di Mitri, D. Gauthier, S. Spampinati, M. Trovó, L. Giannessi, E. Roussel, S. Bettoni, P. Craievich, and E. Ferrari, Passive Linearization of the Magnetic Bunch Compression Using Self-Induced Fields, *Phys. Rev. Lett.* **119**, 184802 (2017).
- [41] A. A. Lutman, T. J. Maxwell, J. P. MacArthur, M. W. Guetg, N. Berrah, R. N. Coffee, Y. Ding, Z. Huang, A. Marinelli, S. Moeller, and J. C. U. Zemella, Fresh-slice multicolour X-ray free-electron lasers, *Nat. Photonics* **10**, 745 (2016).
- [42] S. Bettoni, E. Prat, and S. Reiche, Two-color beam generation based on wakefield excitation, *Phys. Rev. Accel. Beams* **19**, 050702 (2016).
- [43] R. Ischebeck, E. Prat, V. Thominet, and C. Ozkan Loch, Transverse profile imager for ultrabright electron beams, *Phys. Rev. ST Accel. Beams* **18**, 082802 (2015).
- [44] J. Zemella, K. Bane, A. Fisher, M. Guetg, Z. Huang, R. Iverson, P. Krejcik, A. Lutman, T. Maxwell, A. Novokhatski, G. Stupakov, Z. Zhang, M. Harrison, and M. Ruelas, Measurements of wake-induced electron beam deflection in a dechirper at the linac coherent light source, *Phys. Rev. Accel. Beams* **20**, 104403 (2017).
- [45] P. Craievich and A. A. Lutman, Effects of the quadrupole wakefields in a passive streaker, *Nucl. Instrum. Methods Phys. Res., Sect. A* **865**, 55 (2017).
- [46] E. Prat, P. Dijkstal, M. Aiba, S. Bettoni, P. Craievich, E. Ferrari, R. Ischebeck, F. Lohl, A. Malyzhenkov, G. L. Orlandi, S. Reiche, and T. Schietinger, Generation and Characterization of Intense Ultralow-Emittance Electron Beams for Compact X-Ray Free-Electron Lasers, *Phys. Rev. Lett.* **123**, 234801 (2019).
- [47] Z. Huang, K. Bane, Y. Cai, A. Chao, R. Hettel, and C. Pellegrini, Steady-state analysis of short-wavelength, high-gain FELs in a large storage ring, *Nucl. Instrum. Methods Phys. Res., Sect. A* **593**, 120 (2008).
- [48] P. Dijkstal, A. Malyzhenkov, S. Reiche, and E. Prat, Demonstration of two-color x-ray free-electron laser pulses with a sextupole magnet, *Phys. Rev. Accel. Beams* **23**, 030703 (2020).
- [49] K. Tiedtke, J. Feldhaus, U. Hahn, U. Jastrow, T. Nunez, T. Tschentscher, S. V. Bobashev, A. A. Sorokin, J. B. Hastings, S. Möller, L. Cibik, A. Gottwald, A. Hoehl, U. Kroth, M. Krumrey, H. Schöppe, G. Ulm, and M. Richter, Gas detectors for x-ray lasers, *J. Appl. Phys.* **103**, 094511 (2008).
- [50] P. Dijkstal, Data for Self-synchronized cost-effective time-resolved measurements at x-ray free-electron lasers with femtosecond resolution, Zenodo (2021), <http://doi.org/10.5281/zenodo.5744926>.